J. Math. Anal. Appl. • • • (• • • •) • • •–• • •

Contents lists available at ScienceDirect

Journal of Mathematical Analysis and Applications

www.elsevier.com/locate/jmaa

A nonlinear weighted least-squares finite element method for the Carreau–Yasuda non-Newtonian model

Hsueh-Chen Lee [1]

General Education Center, Wenzao Ursuline University of Languages, Kaohsiung, Taiwan

ARTICLE INFO

Article history:
Received 29 March 2015
Available online xxxx
Submitted by W. Layton

Keywords:
Weighted least-squares
Nonlinear weight
Non-Newtonian
Carreau–Yasuda
Shear-thinning

ABSTRACT

We study a nonlinear weighted least-squares finite element method for the Navier–Stokes equations governing non-Newtonian fluid flows by using the Carreau–Yasuda model. The Carreau–Yasuda model is used to describe the shear-thinning behavior of blood. We prove that the least-squares approximation converges to linearized solutions of the non-Newtonian model at the optimal rate. By using continuous piecewise linear finite element spaces for all variables and by appropriately adjusting the nonlinear weighting function, we obtain optimal L^2-norm error convergence rates in all variables. Numerical results are given for a Carreau fluid in the 4-to-1 contraction problem, revealing the shear-thinning behavior. The physical parameter effects are also investigated.

1. Introduction

The objective of this study is to analyze a nonlinear weighted least-squares finite element method for the Carreau–Yasuda non-Newtonian model based on the Navier–Stokes equations. The Carreau–Yasuda model is a popular non-Newtonian model for describing the shear-thinning behavior of blood in hemodynamic simulations [5,16].

Let Ω be an open, connected, and bounded domain in $\mathbb{R}^d$, $d = 2$ or 3 with boundary Γ. The steady-state, incompressible Navier–Stokes equation with the velocity boundary condition can be posed as follows:

$$\begin{aligned} \mathbf{u}\cdot\nabla\mathbf{u} - \nabla\cdot\boldsymbol{\tau} + \nabla p &= \hat{\mathbf{f}} \quad \text{in } \Omega, \\ \boldsymbol{\tau} - \frac{2\eta(\dot{\gamma}(\mathbf{u}))\,\mathbf{D}(\mathbf{u})}{\eta_0 Re} &= \mathbf{0} \quad \text{in } \Omega, \\ \nabla\cdot\mathbf{u} &= 0 \quad \text{in } \Omega, \\ \mathbf{u} &= \mathbf{0} \quad \text{on } \Gamma, \end{aligned} \tag{1}$$

E-mail address: 87013@mail.wzu.edu.tw.

[1] Supported in part by the Ministry of Science and Technology, Taiwan under contract No. 103-2115-M-160-001.

http://dx.doi.org/10.1016/j.jmaa.2015.07.012
0022-247X/

where $\mathbf{D}(\mathbf{u}) = 0.5(\nabla\mathbf{u} + \nabla\mathbf{u}^T)$ is the standard strain rate tensor. $Re \geq 1$ is the Reynolds number, $Re \equiv LU\rho/\eta_0$, in which η_0 is the zero-shear-rate viscosity, L and U are characteristic length and velocity, respectively, and ρ is the density. $\hat{\mathbf{f}}$ is the body force vector, the unknowns $\mathbf{u}$ and $\boldsymbol{\tau}$ are the velocity and the extra-stress tensor, respectively, and p is the scalar pressure. We assume that the pressure p satisfies a zero mean constraint:

$$\int_{\Omega} p dx = 0,$$

in order to assure the uniqueness of pressure [2]. As for the system (1), it is illustrated in [4] that the system is suitable for incompressible non-Newtonian flows when a direct approximation of the extra stress tensor is desired.

Let $\dot{\gamma}(\mathbf{u}) = \sqrt{2\,(\mathbf{D}(\mathbf{u}) : \mathbf{D}(\mathbf{u}))}$ be the shear rate with the double-dot product between two second-order tensors $\boldsymbol{\tau}$ and $\boldsymbol{\sigma}$ defined as

$$\boldsymbol{\tau} : \boldsymbol{\sigma} = \sum_{i,j} \boldsymbol{\tau}_{ij}\boldsymbol{\sigma}_{ji}.$$

We implement the non-Newtonian fluid equation known as the Carreau–Yasuda model [5], i.e.

$$\eta(\dot{\gamma}(\mathbf{u})) = \eta_\infty + (\eta_0 - \eta_\infty)[1 + (\lambda_c\dot{\gamma}(\mathbf{u}))^a]^{\frac{n-1}{a}}, \tag{2}$$

where a, n, and λ_c are determined constant parameters. $a > 0$ is the dimensionless parameter, λ_c is the Carreau time constant, and the parameter n is the power law exponent. In the case of $n = 1$, the model reduces to the linear Newtonian model, i.e. the Navier–Stokes equations. For a shear-thinning fluid, n is less than one, the viscosity decreases by increasing shear rate. At high shear rates, the viscosity of the fluid is η_∞, whereas at low shear rates, the viscosity is η_0. Sample values of the parameters in the Carreau–Yasuda model are given in [1]. They indicate that many concentrated polymer solutions and melts can be obtained for $a = 2$ and $\eta_\infty = 0$. Equation (2), with $a = 2$, is usually referred to as the Carreau equation, and the parameter a is added later by Yasuda; see [1].

Numerous developments using least-squares finite element methods for non-Newtonian fluid flow problems have been made in recent years [4,6,8–12]. Least-squares finite element methods have been reported to offer several theoretical and computational advantages over the Galerkin method for various boundary value problems [2]. Discretization generates an algebraic system that is always symmetric and positive definite, and a single approximating space for all variables can be used for programming least-squares finite element methods [14]. The least-squares functional of the velocity–pressure–stress formulation has the advantage that stress tensor components are computed directly [13]. Hence, the method is suitable for cases in which a direct approximation of the extra stress tensor is necessary (e.g., non-Newtonian fluid flows).

In [4], Bose and Carey present a least-squares method using p-type finite elements and a mesh redistribution for non-Newtonian flows, and indicate the importance of scaling in the original differential equations for the least-squares minimization process. In [14], Lee and Chen propose a nonlinear weighted least-squares (NL-WDLS) method that allows for the use of simple combinations of interpolations, including equal-order linear elements for Stokes equations. They indicate the choice of weights used to balance the residual contributions, and their results show some improvement over the case with no weightings. On the basis of their ideas, NL-WDLS methods based on the velocity–stress–pressure formulation of Stokes equations have been applied to generalized Newtonian and viscoelastic fluid flows in numerical experiments [8,11]. The results indicate that when linear approximations in all variables are employed, the least-squares solutions exhibit numerical convergence rates of $O(h^2)$ in the L^2-norm for all dependent variables (or nearly so for the viscoelastic case). In [12], an adaptively refined least-squares (AR-LS) approach with an inertial term

Please cite this article in press as: H.-C. Lee, A nonlinear weighted least-squares finite element method for the Carreau–Yasuda non-Newtonian model, J. Math. Anal. Appl. (2015), http://dx.doi.org/10.1016/j.jmaa.2015.07.012

is applied to the Carreau model; the least-squares approach uses a grading function of velocity magnitude to adaptively refine the mesh. The results indicate that by using linear approximations in all variables, the resulting convergence rates of the least-squares solutions on uniform grids are not optimal, and those on adaptively refined girds can be restored using adaptive mesh refinements.

On the basis of these studies, we develop a NL-WDLS method for the Carreau–Yasuda non-Newtonian model based on the Navier–Stokes equations. Unlike previous studies based on adaptive grids [12], we consider the NL-WDLS method by using uniform grids. The least-squares functional involved the L^2-norm of the residuals of each equation multiplied by appropriate weights including the mass conservation constant, a mesh dependent, and a nonlinear weighting function. The analysis of error bounds for the NL-WDLS method follows the concept introduced in [2,12,13]. Using continuous piecewise linear finite element spaces for all variables, the numerical solutions exhibit a second-order convergence rate in the L^2-norm. These results show that the additional weighting term does not affect most of the convergence of least-squares finite element methods for the linearized Navier–Stokes equations in [2,12]; however, the expected optimal convergence rates in numerical results can be restored with a careful choice of nonlinear weighting functions. We extend the implementation to simulate the 4-to-1 contraction problem in a range of lower Re numbers ($1 \leq Re \leq 100$) as shown in [4,17] and address the physical parameter effects. In [17], Zinani and Frey present a Galerkin least-squares (GLS) with an equal-order linear interpolation function that adds stabilized formulations to the Carreau model. We show that the results of the NL-WDLS approach are compatible with those of the AR-LS method [12], as well as the reduced GLS method presented by Zinani and Frey in [17]. We also show that the inertial term and viscosity parameter effects become dominant in cases of highly nonlinear viscosity in the non-Newtonian model.

The rest of this paper is organized as follows. Section 2 presents the notation, preliminaries, and ellipticity of the H^{-1} least-squares functional. Section 3 provides the error estimates of the discrete nonlinear weighted L^2 least-squares approximations. Section 4 presents the nonlinear iterative method for approximating the solution of the Navier–Stokes problem with the Carreau–Yasuda model using the nonlinear weighted least-squares approach. Section 5 provides test problems for the flow past a planar channel and 4-to-1 contraction problems, and finally, Section 6 offers concluding remarks.

2. Notation and preliminaries

Let $\mathcal{D}(\Omega)$ be the linear space of infinitely differentiable functions with compact supports on Ω, that is,

$$\mathcal{D}\left(\bar{\Omega}\right) = \{\psi|_{\Omega} : \psi \in \mathcal{D}(\mathcal{O}) \text{ for some open subsect } \Omega \subset \mathcal{O} \subset \mathbb{R}^d\};$$

see [7]. Let $H^s(\Omega)$, $s \geq 0$, be the Sobolev spaces with the standard associated inner products $(\cdot,\cdot)_s$ and their respective norms $\|\cdot\|_s$. For $s = 0$, $H^s(\Omega)$ coincides with $L^2(\Omega)$, and $H_0^s(\Omega)$ denotes the closure of $\mathcal{D}(\Omega)$ with respect to the norm $\|\cdot\|_s$. For positive values of s, the space $H^{-s}(\Omega)$ is defined as the dual space of $H_0^s(\Omega)$ equipped with the norm

$$\|\sigma\|_{-s} := \sup_{0 \neq v \in H_0^s(\Omega)} \frac{(\sigma, v)}{\|v\|_s},$$

where $(.,.)$ is the duality pairing between $H_0^{-s}(\Omega)$ and $H_0^s(\Omega)$ when there is no risk of confusion. Define the product spaces $\mathbf{H}_0^s(\Omega)^d = \prod_{i=1}^d H_0^s(\Omega)$ and $\mathbf{H}_0^{-s}(\Omega)^d = \prod_{i=1}^d H_0^{-s}(\Omega)$. Let $\mathbf{H}(\mathrm{div};\Omega) = \{\boldsymbol{v} \in \mathbf{L}^2(\Omega)^d : \nabla \cdot \boldsymbol{v} \in L^2(\Omega)\}$ with the respective norm $\|\boldsymbol{v}\|_{\mathbf{H}\left(\mathrm{div};\Omega\right)} := (\|\boldsymbol{v}\|_0^2 + \|\nabla \cdot \boldsymbol{v}\|_0^2)^{\frac{1}{2}}$.

The function spaces used in our variational formulations are defined as

$$\boldsymbol{V} := \{\mathbf{v} \mid \mathbf{v} \in \mathbf{H}^1(\Omega)^d,\ \mathbf{v} = \mathbf{0} \text{ on } \partial\Omega\},$$

Please cite this article in press as: H.-C. Lee, A nonlinear weighted least-squares finite element method for the Carreau–Yasuda non-Newtonian model, J. Math. Anal. Appl. (2015), http://dx.doi.org/10.1016/j.jmaa.2015.07.012

$$Q := \{q \mid q \in L^2(\Omega), \int_\Omega q dx = 0\},$$

$$\boldsymbol{\Sigma}_s := \{\boldsymbol{\sigma} \mid \boldsymbol{\sigma} \in \mathbf{L^2}(\Omega)^d,\ \sigma_{ij} = \sigma_{ji}\},$$

and let the product space $\boldsymbol{\Phi} := \boldsymbol{V} \times Q \times \boldsymbol{\Sigma}_s$.

Based on [12], linearizing (1) about the approximation

$$\mathbf{u}_0 \approx \mathbf{u},$$

where we assume

$$\nabla \cdot \mathbf{u}_0 = 0, \tag{3}$$

and

$$M = \max\{\|\mathbf{u}_0\|_\infty,\ \|\nabla \mathbf{u}_0\|_\infty\} < \infty, \tag{4}$$

results in the following replacement rules:

$$\mathbf{u} \cdot \nabla \mathbf{u} \approx \mathbf{u}_0 \cdot \nabla \mathbf{u} + \mathbf{u} \cdot \nabla \mathbf{u}_0 - \mathbf{u}_0 \cdot \nabla \mathbf{u}_0,$$
$$\eta(\dot\gamma(\mathbf{u}))\mathbf{D}(\mathbf{u}) \approx \eta(\dot\gamma(\mathbf{u}_0))\mathbf{D}(\mathbf{u}) + \eta(\dot\gamma(\mathbf{u}))\mathbf{D}(\mathbf{u}_0) - \eta(\dot\gamma(\mathbf{u}_0))\mathbf{D}(\mathbf{u}_0),$$

and

$$\eta(\dot\gamma(\mathbf{u}_0)) \approx \eta_0.$$

As stated in [12], we apply Newton's method to the nonlinear viscosity equation (2). Let $\mathbf{u} = \tilde{\mathbf{u}} + \mathbf{u}_0$, where $\mathbf{u}_0$ is the initial guess and $\tilde{\mathbf{u}}$ is the correction in the Newton iteration. A binomial expansion of $\eta(\dot\gamma(\mathbf{u}_0 + \epsilon\tilde{\mathbf{u}}))$ yields the equation

$$\eta(\dot\gamma(\mathbf{u}_0 + \epsilon\tilde{\mathbf{u}})) = \eta(\dot\gamma(\mathbf{u}_0))\left[1 + \epsilon G(\mathbf{u}_0, \tilde{\mathbf{u}}) + O(\epsilon^2)\right], \tag{5}$$

where

$$G(\mathbf{u}_0, \tilde{\mathbf{u}}) = 2^{\frac{a}{2}}(n-1)\lambda_c^a(\mathbf{D}(\mathbf{u}_0) : \mathbf{D}(\mathbf{u}_0))^{\frac{(a-2)}{2}} \frac{(\mathbf{D}(\mathbf{u}_0) : \mathbf{D}(\tilde{\mathbf{u}}))}{1 + \lambda_c^a[\dot\gamma(\mathbf{u}_0)]^a}. \tag{6}$$

Hence,

$$\eta(\dot\gamma(\mathbf{u})) \approx \eta_0\left[1 + G(\mathbf{u}_0, \mathbf{u}) - G(\mathbf{u}_0, \mathbf{u}_0)\right]. \tag{7}$$

The linearized velocity–pressure–stress system may now be written as

$$\mathbf{u}_0 \cdot \nabla \mathbf{u} + \mathbf{u} \cdot \nabla \mathbf{u}_0 - \nabla \cdot \boldsymbol{\tau} + \nabla p = \mathbf{f} \ \text{ in } \Omega, \tag{8}$$

$$\boldsymbol{\tau} - \frac{2}{Re}\mathbf{D}(\mathbf{u}) - \frac{2}{Re}\mathbf{D}(\mathbf{u}_0)G(\mathbf{u}_0, \mathbf{u}) = \mathbf{g} \ \text{ in } \Omega, \tag{9}$$

$$\nabla \cdot \mathbf{u} = 0 \ \text{ in } \Omega, \tag{10}$$

$$\mathbf{u} = \mathbf{0} \ \text{ on } \Gamma, \tag{11}$$

where we define

Please cite this article in press as: H.-C. Lee, A nonlinear weighted least-squares finite element method for the Carreau–Yasuda non-Newtonian model, J. Math. Anal. Appl. (2015), http://dx.doi.org/10.1016/j.jmaa.2015.07.012

$$\mathbf{f} = \mathbf{u}_0 \cdot \nabla \mathbf{u}_0 + \hat{\mathbf{f}},$$
$$\mathbf{g} = \frac{-2}{Re}\mathbf{D}(\mathbf{u}_0) G(\mathbf{u}_0, \mathbf{u}_0).$$

The standard least-squares functional for (8)–(11) is given by

$$\begin{aligned} &J(\mathbf{u}, p, \boldsymbol{\tau}; \mathbf{F}) \\ &= \|\mathbf{u}_0 \cdot \nabla \mathbf{u} + \mathbf{u} \cdot \nabla \mathbf{u}_0 - \nabla \cdot \boldsymbol{\tau} + \nabla p - \mathbf{f}\|_{-1}^2 \\ &+ \left\| \boldsymbol{\tau} - \frac{2}{Re}\mathbf{D}(\mathbf{u}) - \frac{2\mathbf{D}(\mathbf{u}_0)}{Re} G(\mathbf{u}_0, \mathbf{u}) - \mathbf{g} \right\|_0^2 + \frac{1}{Re^2} \|\nabla \cdot \mathbf{u}\|_0^2 . \end{aligned} \tag{12}$$

Define the norm

$$|||(\mathbf{u}, p, \boldsymbol{\tau})||| = \left(\|\boldsymbol{\tau}\|_0^2 + \|p\|_0^2 + \frac{1}{Re^2} \|\mathbf{u}\|_1^2 \right)^{1/2},$$

over $\boldsymbol{\Phi}$. In [13], Lee presents the standard H^{-1} least-squares functional J_s for the velocity–pressure–stress formulation of the linearized Navier–Stokes equations as follows

$$\begin{aligned} J_s(\mathbf{u}, p, \boldsymbol{\tau}; \mathbf{F}) &= \|\mathbf{u}_0 \cdot \nabla \mathbf{u} + \mathbf{u} \cdot \nabla \mathbf{u}_0 - \nabla \cdot \boldsymbol{\tau} + \nabla p - \mathbf{f}\|_{-1}^2 \\ &+ \left\| \boldsymbol{\tau} - \frac{2}{Re}\mathbf{D}(\mathbf{u}) \right\|_0^2 + \frac{1}{Re^2} \|\nabla \cdot \mathbf{u}\|_0^2 , \end{aligned} \tag{13}$$

and establishes the following a priori error estimate,

$$C|||(\mathbf{u}, p, \boldsymbol{\tau})|||^2 \le J_s(\mathbf{u}, p, \boldsymbol{\tau}; \mathbf{0}) \le C|||(\mathbf{u}, p, \boldsymbol{\tau})|||^2, \tag{14}$$

for M in (4) satisfying

$$M \le \frac{1}{2Re}, \tag{15}$$

and $C > 0$ independent of Re, $\forall (\mathbf{u}, p, \boldsymbol{\tau}) \in \boldsymbol{\Phi}$.

Based on [12] and using (14), we now derive some a priori estimates for the first-order system (8)–(11). The a priori estimates will play the crucial roles in the error estimates of our least-squares finite element method.

Theorem 1. *For any $(\mathbf{u}, p, \boldsymbol{\tau}) \in \boldsymbol{\Phi}$, there are positive constants, c_0 and c_1, which depend on Ω, n, λ_c and M in (4), such that*

$$c_0|||(\mathbf{u}, p, \boldsymbol{\tau})|||^2 \le J(\mathbf{u}, p, \boldsymbol{\tau}; \mathbf{0}) \le c_1|||(\mathbf{u}, p, \boldsymbol{\tau})|||^2, \tag{16}$$

for sufficiently small M in Ω satisfying

$$M \le \frac{1}{2Re}. \tag{17}$$

Proof. Let $(\mathbf{u}, p, \boldsymbol{\tau}) \in \boldsymbol{\Phi}$. The upper bound follows naturally from the triangle inequality. Using the inequality $\|a + b\|^2 \ge (1/2)\|a\|^2 - |b\|^2$ and the estimate (14) with (15), we have

Please cite this article in press as: H.-C. Lee, A nonlinear weighted least-squares finite element method for the Carreau–Yasuda non-Newtonian model, J. Math. Anal. Appl. (2015), http://dx.doi.org/10.1016/j.jmaa.2015.07.012

$$
\begin{aligned}
&J(\mathbf{u},p,\boldsymbol{\tau};\mathbf{0})\\
&\geq \frac{1}{2}\left(J_s(\mathbf{u},p,\boldsymbol{\tau};\mathbf{0})\right)-\frac{4\|\mathbf{D}(\mathbf{u}_0)\|^2}{Re^2}\|G\left(\mathbf{u}_0,\mathbf{u}\right)\|_0^2\\
&\geq \frac{1}{2}\left(|||(\mathbf{u},p,\boldsymbol{\tau})|||^2\right)-C_1(n-1)^2\lambda_c^{2a}Re^{-2}M^{a+2}\|\mathbf{u}\|_1^2\\
&\geq C_2\left(\|\boldsymbol{\tau}\|_0^2+\|p\|_0^2+\frac{1}{Re^2}\|\mathbf{u}\|_1^2\left(1-M^{a+2}\right)\right). \qquad (18)
\end{aligned}
$$

By using (17), we have $1-M^{a+2}>0$. Hence,

$$J(\mathbf{u},p,\boldsymbol{\tau};\mathbf{0})\geq c_0|||(\mathbf{u},p,\boldsymbol{\tau})|||^2,$$

for some positive constant c_0 which is independent of Re. □

Therefore, the coercivity and continuity estimates of the functional $J(\mathbf{u},p,\boldsymbol{\tau};\mathbf{0})$ have been established in Theorem 1. The least-squares minimization problem for the solution of system (8)–(11) is to choose $(\mathbf{u},p,\boldsymbol{\tau})\in\boldsymbol{\Phi}$ such that

$$J(\mathbf{u},p,\boldsymbol{\tau};\mathbf{F})=\inf_{(\mathbf{v},q,\boldsymbol{\sigma})\in\boldsymbol{\Phi}}J(\mathbf{v},q,\boldsymbol{\sigma};\mathbf{F}). \qquad (19)$$

The ellipticity of the functional J has been established in Theorem 1, but the H^{-1} least-squares functional is not practical in the computation. Based on [2,13,14], the mesh dependent L^2 least-squares functional will be considered in the work.

3. A nonlinear weighted least-squares functional

In this section, we define and analyze weighted least-squares methods for the approximate solutions of (8)–(11). For the finite element approximation, we assume that the domain Ω is a polygon for $d=2$ or a polyhedron for $d=3$, and that Γ_h is a regular triangulation of the domain Ω, as $\Omega=\bigcup_{T\in\Gamma_h}T$ with $h=\max\{\mathrm{diam}(T):T\in\Gamma_h\}$ (see [13]). Let $P_r(T)$ denote the space of polynomials with the degree less than or equal to r defined over T. Define finite element spaces for the approximate of $(\mathbf{u},p,\boldsymbol{\tau})$:

$$
\begin{aligned}
\boldsymbol{V}^h&=\{\mathbf{v}^h\mid\mathbf{v}^h\in\mathbf{V}\cap(C^0(\Omega))^d,\ \mathbf{v}^h|_T\in P_r(T)^d,\ \forall T\in\Gamma_h\},\\
Q^h&=\{q^h\mid q^h\in Q\cap C^0(\Omega),\ q^h|_T\in P_r(T),\ \forall T\in\Gamma_h\},\\
\boldsymbol{\Sigma}_s^h&=\{\boldsymbol{\sigma}_s^h\mid\boldsymbol{\sigma}_s^h\in\boldsymbol{\Sigma}_s\cap(C^0(\Omega))^{2d},\ \boldsymbol{\sigma}_s^h|_T\in P_r(T)^{2d},\ \forall T\in\Gamma_h\}.
\end{aligned}
$$

Let $\boldsymbol{\Phi}^h:=\mathbf{V}^h\times Q^h\times\boldsymbol{\Sigma}_s^h$ be finite element subspaces of $\boldsymbol{\Phi}$ with the following approximation prosperities: there exists a positive integer r such that the spaces S_j approximate optimally with respect to the space $H^{r+j}(\Omega)$, $j=1,\ 2$. More precisely, we assume that for all $u\in H^{r+j}(\Omega)$ there exists an element $u^I\in S_j$ such that $0\leq m\leq 1$,

$$\left\|u-u^I\right\|_m\leq Ch^{r+j-m}\|u\|_{r+j}, \qquad (20)$$

and the spaces S_j satisfy the inverse assumption, i.e. that

$$\left\|v^h\right\|_1\leq Ch^{-1}\left\|v^h\right\|_0,\ \forall v^h\in S_j. \qquad (21)$$

We can consider the nonlinear weighted least-squares functional associated with the first-order system (8)–(11):

Please cite this article in press as: H.-C. Lee, A nonlinear weighted least-squares finite element method for the Carreau–Yasuda non-Newtonian model, J. Math. Anal. Appl. (2015), http://dx.doi.org/10.1016/j.jmaa.2015.07.012

$$
\begin{aligned}
&J^h(\mathbf{u}, p, \boldsymbol{\tau}; \mathbf{F}) \\
&= h^2 \left\| \mathbf{u}_0 \cdot \nabla \mathbf{u} + \mathbf{u} \cdot \nabla \mathbf{u}_0 - \nabla \cdot \boldsymbol{\tau} + \nabla p - \mathbf{f} \right\|_0^2 \\
&+ \left\| w_s(\mathbf{u}_0) \left(\boldsymbol{\tau} - \frac{2}{Re} \mathbf{D}(\mathbf{u}) - \frac{2\mathbf{D}(\mathbf{u}_0)}{Re} G(\mathbf{u}_0, \mathbf{u}) - \mathbf{g} \right) \right\|_0^2 + \frac{1}{Re^2} \left\| \nabla \cdot \mathbf{u} \right\|_0^2,
\end{aligned} \tag{22}
$$

over all $\mathbf{u} \in \boldsymbol{V}^h$, $p \in Q^h$, and $\boldsymbol{\tau} \in \boldsymbol{\Sigma}_s^h$. In (22), the weight h^2 and the function w_s are chosen based on similar considerations as those used in [13,14]. The weight w_s in (22) indicates that the nonlinear weight w_s is evaluated at $\mathbf{u}_0$. The nonlinear weight function w_s is defined in each element as

$$
w_s(\mathbf{u}) = \frac{1}{\sqrt{1 + (\dot{\gamma}(\mathbf{u}))^2}}. \tag{23}
$$

Based on [3,12,13] and application of Theorem 1, we establish error estimates of a discrete least-squares finite element functional as follows.

We have the following inequality (cf. [3, p. 583]):

Lemma 1. *Assume that Ω is a bounded open region in $\Omega \subset \mathbb{R}^d$, $d = 2$ or $d = 3$ and $\mathcal{T}_h$ is a uniformly regular partition of Ω into finite elements. Then there exists a constant $C > 0$, independent of h, such that, for all $u \in L^2(\Omega)$,*

$$
C^{-1} \|u\|_{-1} \leq C(h\|u\|_0 + \|u\|_{-1}). \tag{24}
$$

If, in addition, $0 < C < 1$, then (24) can be replaced by

$$
\|u\|_{-1} \leq \frac{C^2}{1 - C^2}(h\|u\|_0). \tag{25}
$$

Lemma 2. *For any $(\mathbf{u}, p, \boldsymbol{\tau}) \in \boldsymbol{\Phi}^h$, there exist positive constants c and C, independent of h, such that*

$$
c|||(\mathbf{u}, p, \boldsymbol{\tau})|||^2 \leq J^h(\mathbf{u}, p, \boldsymbol{\tau}; \mathbf{0}) \leq C|||(\mathbf{u}, p, \boldsymbol{\tau})|||^2, \tag{26}
$$

for any $h < 1$ and sufficiently small values of M in (4) satisfying (17).

Proof. Let $(\mathbf{u}, \boldsymbol{\tau}, p) \in \boldsymbol{\Phi}^h$. The upper bound is naturally obtained from the triangle inequality and the inverse inequalities

$$
\|\nabla \cdot \boldsymbol{\tau}\|_0 \leq Ch^{-1} \|\boldsymbol{\tau}\|_0, \ \|\nabla p\|_0 \leq Ch^{-1} \|p\|_0.
$$

Application of Theorem 1 and Lemma 1 yields the estimate

$$
\begin{aligned}
&c|||(\mathbf{u}, p, \boldsymbol{\tau})|||^2 \\
&\leq \left\| \boldsymbol{\tau} - \frac{2}{Re} \mathbf{D}(\mathbf{u}) - \frac{2\mathbf{D}(\mathbf{u}_0)}{\eta_0 Re} G(\mathbf{u}_0, \mathbf{u}) \right\|_0^2 + Re^{-2} \|\nabla \cdot \mathbf{u}\|_0^2 \\
&+ h^2 \|\mathbf{u}_0 \cdot \nabla \mathbf{u} + \mathbf{u} \cdot \nabla \mathbf{u}_0 - \nabla \cdot \boldsymbol{\tau} + \nabla p\|_0^2 \\
&\leq C_1 \left\| w_s(\mathbf{u}_0) \left(\boldsymbol{\tau} - \frac{2}{Re} \mathbf{D}(\mathbf{u}) - \frac{2\mathbf{D}(\mathbf{u}_0)}{\eta_0 Re} G(\mathbf{u}_0, \mathbf{u}) \right) \right\|_0^2 + Re^{-2} \|\nabla \cdot \mathbf{u}\|_0^2 \\
&+ h^2 \|\mathbf{u}_0 \cdot \nabla \mathbf{u} + \mathbf{u} \cdot \nabla \mathbf{u}_0 + \nabla \cdot \boldsymbol{\tau} + \nabla p\|_0^2,
\end{aligned}
$$

for $C_1 = 2\max\{1, 2M^2\}\,|\Omega|$ with $(\dot{\gamma}(\mathbf{u}_0))^2 \leq 2M^2 < \infty$ using (4). Hence, the lower bound is established. □

Please cite this article in press as: H.-C. Lee, A nonlinear weighted least-squares finite element method for the Carreau–Yasuda non-Newtonian model, J. Math. Anal. Appl. (2015), http://dx.doi.org/10.1016/j.jmaa.2015.07.012

The discrete least-squares minimization problem for the solution of system (8)–(11) is to choose $(\mathbf{u}^h, p^h, \boldsymbol{\tau}^h) \in \boldsymbol{\Phi}^h$ such that

$$J^h(\mathbf{u}^h, p^h, \boldsymbol{\tau}^h; \mathbf{F}) = \inf_{(\mathbf{v}^h, q^h, \boldsymbol{\sigma}^h) \in \boldsymbol{\Phi}^h} J^h(\mathbf{v}^h, q^h, \boldsymbol{\sigma}^h; \mathbf{F}). \tag{27}$$

Since $\boldsymbol{\Phi}^h$ is a finite element subspace of $\boldsymbol{\Phi}$, using Theorem 1, Lemma 2, and the Lax–Milgram lemma, the following theorem is proved.

Theorem 2. *The least-squares functional (22) has the unique minimizer out of the space $\boldsymbol{\Phi}^h$ for any $h < 1$ and sufficiently small M.*

Using similar arguments as in [12] and the approximation properties (20), the following error estimate is established.

Theorem 3. *Let $U = (\mathbf{u}, p, \boldsymbol{\tau}) \in \boldsymbol{\Phi}$ be the solution of the problem (8)–(11) and $U^h = (\mathbf{u}^h, p^h, \boldsymbol{\tau}^h) \in \boldsymbol{\Phi}^h$ denote the solution of the variational problem (27). Then there exists a constant C, independent of the mesh size h and Re, such that*

$$|||(\mathbf{u} - \mathbf{u}^h, p - p^h, \boldsymbol{\tau} - \boldsymbol{\tau}^h)||| \le Ch^{r+1} \left(\|\boldsymbol{\tau}\|_{r+1} + \|p\|_{r+1} + \frac{1}{Re} \|\mathbf{u}\|_{r+2} \right), \tag{28}$$

under the assumptions in (4) and (17).

Under some assumptions, the error in (28) is of the same order as the error in the least-squares solutions of the linearized Navier–Stokes equations [13]. Note that the use of continuous piecewise linear polynomials for all unknowns yields the convergence rates,

$$\|\boldsymbol{\tau} - \boldsymbol{\tau}^h\|_0 = O(h), \ \|p - p^h\|_0 = O(h), \text{ and } \|\mathbf{u} - \mathbf{u}^h\|_1 = O(h).$$

The theoretically predicted error bounds are only $O(h)$ in the L^2-norm for p and $\boldsymbol{\tau}$ and $O(h)$ in the H^1-norm for $\mathbf{u}$. Hence, we have the optimal convergence rate of the velocity in the H^1-norm and suboptimal convergence rates of the stress and pressure in the L^2-norm.

4. Nonlinear iterative method

In this section, we present a Newton iteration scheme for solving Navier–Stokes equations by using a nonlinear weighted least-squares method. The unknowns are denoted as $U = (\mathbf{u}, p, \boldsymbol{\tau}) \in \boldsymbol{\Phi}$ and the steady state residual of the system (1) is denoted as

$$\mathbf{R}(U) := \begin{bmatrix} \mathbf{u} \cdot \nabla \mathbf{u} - \nabla \cdot \boldsymbol{\tau} + \nabla p - \mathbf{f} \\ \boldsymbol{\tau} - (2/Re)(\eta/\eta_0)\mathbf{D}(\mathbf{u}) - \mathbf{g} \\ \nabla \cdot \mathbf{u} \end{bmatrix}.$$

We now approximate the solution to $\mathbf{B}(U) := \mathbf{P}^{\mathrm{T}}\mathbf{R}(U) = \mathbf{0}$ with a diagonal matrix $\mathbf{P}$ whose diagonal entries consist of least-squares weighting functions for the momentum, constitutive, and continuity equations by an inexact Newton iteration. The ℓth iterate approximated on Ω is given by U_ℓ. Each linear step in this iterative procedure is found by solving for the update $S_\ell = U_{\ell+1} - U_\ell$ in the linear problem

$$\mathbf{J}(U_\ell) S_\ell = -\mathbf{B}(U_\ell), \tag{29}$$

Please cite this article in press as: H.-C. Lee, A nonlinear weighted least-squares finite element method for the Carreau–Yasuda non-Newtonian model, J. Math. Anal. Appl. (2015), http://dx.doi.org/10.1016/j.jmaa.2015.07.012

where $\mathbf{J}$ is the Jacobian of $\mathbf{B}$. The new approximation is given by $U_{\ell+1} = U_\ell + S_\ell$. Each linear problem (29) is cast as a least-squares minimization problem by defining the linear least-squares functional

$$J_\ell^h(S_\ell) = \|\mathbf{J}(U_\ell)S_\ell + \mathbf{B}(U_\ell)\|^2,$$

and then finding $S_\ell \in \mathbf{\Phi}^h$ such that

$$J_\ell^h(S_\ell) \leq J_\ell^h(V_\ell)\ \forall V_\ell \in \mathbf{\Phi}^h.$$

The solution of the nonlinear systems in (1) is approximated by a sequence of the linearized system (8)–(11). Then the least-squares approach to the linearized system (8)–(11) provides an iterative procedure as follows. We give an initial approximation $U_0^h = (\mathbf{u}_0^h, p_0^h, \boldsymbol{\tau}_0^h)$ and then attempt to seek approximations $U_{\ell+1}^h = (\mathbf{u}_{\ell+1}^h, p_{\ell+1}^h, \boldsymbol{\tau}_{\ell+1}^h) \in \mathbf{\Phi}^h$ for $\ell = 0,\ 1,\ 2,\ \ldots$ satisfying

$$J_\ell^h(\mathbf{u}_{\ell+1}^h, p_{\ell+1}^h, \boldsymbol{\tau}_{\ell+1}^h; \mathbf{F}) = \inf_{V_\ell = (\mathbf{v}^h, q^h, \boldsymbol{\sigma}^h) \in \mathbf{\Phi}^h} J_\ell^h(\mathbf{v}^h, q^h, \boldsymbol{\sigma}^h; \mathbf{F}), \tag{30}$$

where the nonlinear weighted least-squares (NL-WDLS) functional $J_\ell^h(\mathbf{u}, p, \boldsymbol{\tau}; \mathbf{F})$ is defined as

$$\begin{aligned} J_\ell^h(\mathbf{u}, p, \boldsymbol{\tau}; \mathbf{F}) = {} & h^2 \left\| \mathbf{u}_\ell^h \cdot \nabla \mathbf{u} + \mathbf{u} \cdot \nabla \mathbf{u}_\ell^h - \nabla \cdot \boldsymbol{\tau} + \nabla p - \mathbf{f} \right\|_0^2 + KRe^{-2} \left\| \nabla \cdot \mathbf{u} \right\|_0^2 \\ & + \left\| w_s(\mathbf{u}_\ell^h)(\boldsymbol{\tau} - \frac{2}{Re}\mathbf{D}(\mathbf{u}) - \frac{2}{Re}\mathbf{D}(\mathbf{u}_\ell^h) G\left(\mathbf{u}_\ell^h, \mathbf{u}\right) - \mathbf{g}) \right\|_0^2, \end{aligned} \tag{31}$$

where

$$\begin{aligned} \mathbf{f} &= \mathbf{u}_\ell^h \cdot \nabla \mathbf{u}_\ell^h + \widehat{\mathbf{f}}, \\ \mathbf{g} &= \frac{-2}{Re}\mathbf{D}(\mathbf{u}_\ell^h) G\left(\mathbf{u}_\ell^h, \mathbf{u}_\ell^h\right), \end{aligned}$$

over the space Φ^h. In our calculation, stabilization parameters h^2, KRe^{-2}, and w_s represent the least-squares weighting functions for the momentum, continuity, and constitutive equations, respectively, as shown in [10,13]. The h^2-term stabilizes the least-squares form in the momentum equation, and replaces the H^{-1}-norm by the L^2-norm. The mass conservation weight K improves the convergence of non-linear solvers in the problem; where the positive constant $K = 10^m$, where m ranges from 1 to 8, is selected based on [8,11]. These results indicate that the ranges of m vary with the problems, and setting K is sufficient to obtain satisfactory results. The nonlinear weighting function w_s stabilizes the least-squares form in the constitutive equation and improves convergence rates over the case of no weighting in Section 5.

5. Test problems

We now consider the flow of the Carreau–Yasuda model with $a = 1$ and $a = 2$ in the planar channel and the 4-to-1 contraction problems. Two physical domains are symmetric along the centerline of each channel, and the one-half domains are used in our computation for efficiency. Both cases presented here use linear basis functions for all variables. All calculations are conducted in a computing environment using the C programming language.

Results of the least-squares method are generated for three versions of (31): with linear weighting depending only on K and Re outside of the norms (LS), with linear weighting depending on h, K, and Re outside of the norms (WDLS), and with all weights (NL-WDLS). The resulting linear algebraic system of equations with a symmetric positive-definite coefficient matrix is solved using the Gaussian elimination method.

Please cite this article in press as: H.-C. Lee, A nonlinear weighted least-squares finite element method for the Carreau–Yasuda non-Newtonian model, J. Math. Anal. Appl. (2015), http://dx.doi.org/10.1016/j.jmaa.2015.07.012

Convergence of the iteration scheme in (31) is declared when the relative norm of the residual in velocities $\|\mathbf{u}^h_{\ell+1} - \mathbf{u}^h_{\ell}\|/\|\mathbf{u}^h_{\ell+1}\|$ between two consecutive iterations is less than 10^{-4}. In general, the approximation solution is achieved within 4 iterations.

Two test problems are considered for the Newtonian model in [13]. In [13], we display the least-squares solutions by using the mass conservation weights $K = 10^m$, where m ranges from 1 to 8 for both cases. The results show that we obtain satisfactory least-squares solutions for all variables with $K \geq 10^2$ in the planar channel problem and $K \geq 10^6$ in the 4-to-1 contraction channel problem. Therefore, it is sufficient to use $K = 10^2$ for Problem 1 and $K = 10^6$ for Problem 2 in (31).

5.1. Problem 1: flow in the planar channel

The first problem is a square test domain with exact boundary conditions and non-zero right-hand sides determined by the exact solutions used to measure convergence rates. For numerical tests, consider the flow in a planar channel on the square domain $[0, 1] \times [0, 1]$, where we have a line of symmetry along $y = 0$. The velocity $\mathbf{u} = [u, v]^T$ is specified on the inflow, outflow, and wall boundaries. On the symmetry boundary, the v and τ_{xy} vanish. The pressure p is specified at the intersection of the wall and outflow boundaries. Smooth exact solutions are given in [12] by

$$\mathbf{u}_{exact} = \begin{bmatrix} 1 - y^4 \\ 0 \end{bmatrix}$$

and

$$p_{exact} = -x^2.$$

The exact solution for the extra-stress tensor is calculated using

$$\boldsymbol{\tau}_{exact} = \frac{1}{Re} \left(2\eta \left(\dot{\gamma}(\mathbf{u}_{exact})\right) \mathbf{D}(\mathbf{u}_{exact})\right).$$

A forcing function, $\mathbf{f}$, must be added to the momentum equation, specifically

$$\mathbf{f} = \begin{bmatrix} \frac{1}{Re}\left(12y^2\left(1 + 4^a n \lambda_c^a y^{3a}\right)\left(1 + (4\lambda_c y^3)^a\right)^{\frac{n-1-a}{a}}\right) - 2x \\ 0 \end{bmatrix}.$$

In the convergence results, the constitutive equation parameters in (2) are set as $\eta_0 = 1$, $\eta_\infty = 0$, $n = 0.1$, $\lambda_c = 1$, and $Re = 1$. Three uniform directional triangular meshes are verified from 8×8, 16×16 to 32×32 and used for all calculations as shown in [13]. We verify these least-squares methods for the Carreau–Yasuda model at $a = 1$ and 2, and show the errors of these least-squares solutions in Figs. 1 and 2, respectively. Figs. 1 ($a = 1$) and 2 ($a = 2$) show optimal convergence rates in L^2-norm and H^1-norm for $\mathbf{u}$ and at least suboptimal convergence rates in L^2-norm for p and $\boldsymbol{\tau}$. This is consistent with our analysis for the least-squares method in Section 3. However, some improvements are seen when using the WDLS method over the LS method. The NL-WDLS method improves convergence rates over the WDLS method in p and $\boldsymbol{\tau}$ from 2 to 2.3 and 1.8 to 2, respectively. We obtain optimal convergence rate of the NL-WDLS solutions for all variables. The convergence rates for $\boldsymbol{\tau}$ and p are better than those of the theoretically predicted $O(h)$ in L^2-norm. Our results show the expected optimal convergence rates in L^2-norm of $O(h^2)$ for all variables can be restored with a careful choice of nonlinear weighting functions.

5.2. Problem 2: flow in the 4-to-1 contraction channel

The second domain is the 4-to-1 contraction channel problem consisting of an upstream channel that abruptly narrows to a one quarter channel of the original width. For the 4-to-1 contraction domain, the

Please cite this article in press as: H.-C. Lee, A nonlinear weighted least-squares finite element method for the Carreau–Yasuda non-Newtonian model, J. Math. Anal. Appl. (2015), http://dx.doi.org/10.1016/j.jmaa.2015.07.012

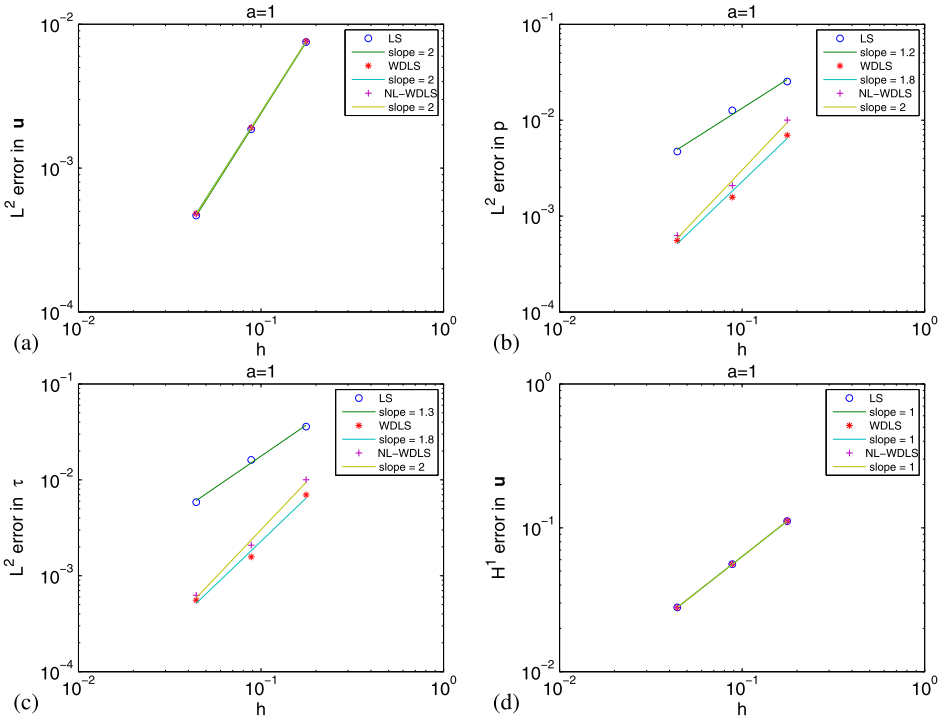

Fig. 1. $a = 1$. L^2 errors in (a) $\mathbf{u}$, (b) p, (c) $\boldsymbol{\tau}$, and (d) H^1 errors in $\mathbf{u}$ of LS (o), WDLS (*), and NL-WDLS (+) solutions at $Re = 1$, $\lambda_c = 1$, and $n = 0.1$.

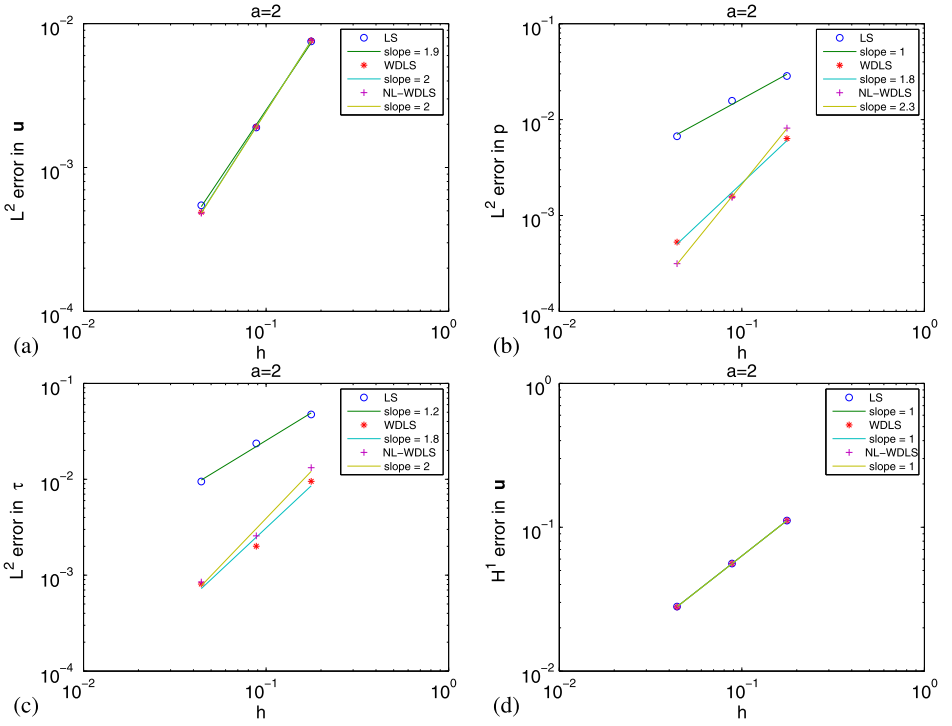

Fig. 2. $a = 2$. L^2 errors in (a) $\mathbf{u}$, (b) p, (c) $\boldsymbol{\tau}$, and (d) H^1 errors in $\mathbf{u}$ of LS (o), WDLS (*), and NL-WDLS (+) solutions at $Re = 1$, $\lambda_c = 1$, and $n = 0.1$.

Please cite this article in press as: H.-C. Lee, A nonlinear weighted least-squares finite element method for the Carreau–Yasuda non-Newtonian model, J. Math. Anal. Appl. (2015), http://dx.doi.org/10.1016/j.jmaa.2015.07.012

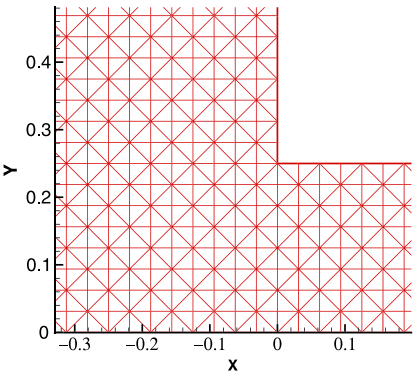

Fig. 3. Union Jack grids with a minimum mesh spacing of 0.03125.

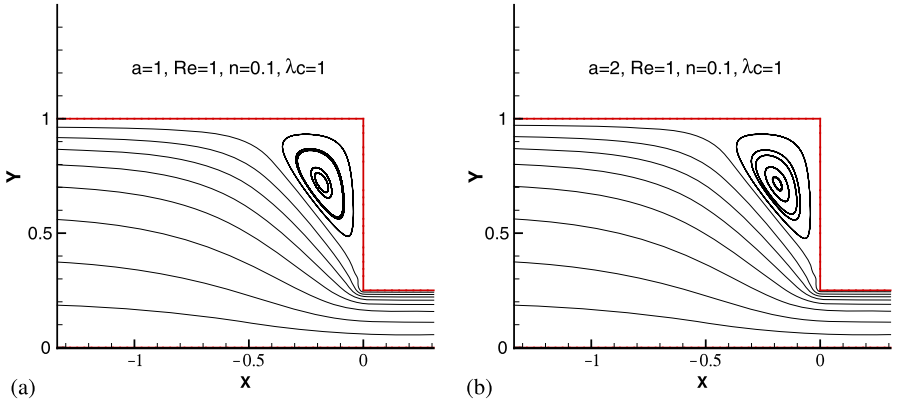

Fig. 4. Streamlines in the Carreau–Yasuda models at (a) $a = 1$ and (b) $a = 2$ for $Re = 1$, $n = 0.1$, and $\lambda_c = 1$.

velocity $\mathbf{u} = [u, v]^T$ is specified on the inflow and wall boundaries. On the symmetry boundary, the v and τ_{xy} vanish. The pressure $p = 0$ and the $v = 0$ are specified on the outflow boundary. These boundary conditions are also used in [12,13].

To further show the NL-WDLS scheme's capability, we applied the method using uniform grids to the 4-to-1 contraction channel with x (the flow direction) varying as $-r \leq x \leq r$, $r = 10$, and the contraction occurring at $x = 0$. The upstream channel width is 1, thus the downstream width is 1/4. In [13], using the Union Jack grids with a minimum mesh spacing of 0.03125 as shown in Fig. 3, we employ the NL-WDLS method to the Newtonian model, and obtain convergence profiles of the horizontal velocity for the 4-to-1 contraction problem. Therefore, in our computations, the uniform Union Jack grid is considered as the uniform mesh next.

The Carreau–Yasuda equation (2) involves five parameters (η_0, η_∞, λ_c, n, a) to describe the fluid rheology. In our calculation, these parameters in (2) are set as $\eta_0 = 1$ and $\eta_\infty = 0$, and four dimensionless parameters are needed to define the flow: parameters a, power-law indices n, Carreau time numbers λ_c, and Reynolds numbers Re. n and λ_c dominate the nonlinear viscosity, and Re dominates the inertia effects. For the dimensionless parameter a, we evaluate the effects of the parameter a on the streamline patterns in Fig. 4. Figs. 4(a) and 4(b) present the streamline patterns of $a = 1$ and $a = 2$ for $Re = 1$, $n = 0.5$, and $\lambda_c = 1$, respectively. The results show that the size of the corner vortex for the two a cases is similar and causes a light increase as a increases. Therefore, the case of $a = 2$ is considered next.

To illustrate capability of these least-squares finite element formulations, we present the streamline patterns of two weighted cases, WDLS and NL-WDLS formulations for $Re = 1$, $n = 0.5$, and $\lambda_c = 1$ in Fig. 5. The results show that in comparison with the NL-WDLS solution, the recirculation zone of fluid in the WDLS solution seems too large. The NL-WDLS results agree with the AR-LS results [12], outperform the

Please cite this article in press as: H.-C. Lee, A nonlinear weighted least-squares finite element method for the Carreau–Yasuda non-Newtonian model, J. Math. Anal. Appl. (2015), http://dx.doi.org/10.1016/j.jmaa.2015.07.012

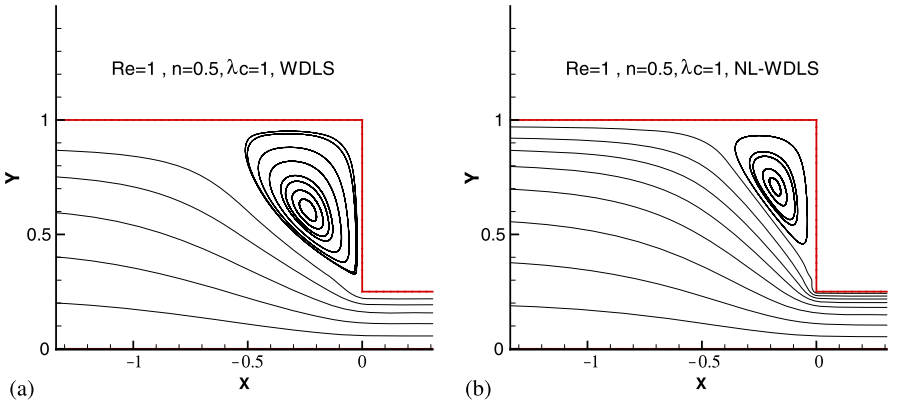

Fig. 5. Streamlines in (a) WDLS and (b) NL-WDLS solutions for $Re = 1$, $n = 0.5$, and $\lambda_c = 1$.

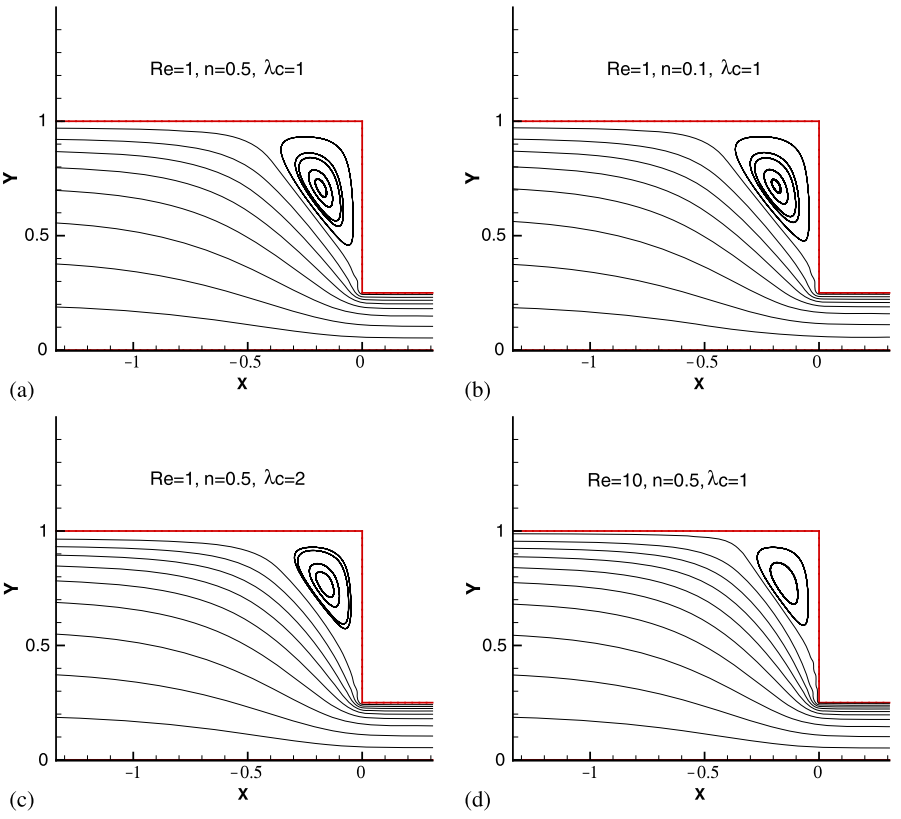

Fig. 6. Streamlines in NL-WDLS solutions at (a) $Re = 1$, $n = 0.5$, $\lambda_c = 1$, (b) $Re = 1$, $n = 0.1$, $\lambda_c = 1$, (c) $Re = 1$, $n = 0.5$, $\lambda_c = 2$, and (d) $Re = 10$, $n = 0.5$, $\lambda_c = 1$.

WDLS method, and yield results which are compatible to those presented in [12]. Therefore, the NL-WDLS functional (31) is considered for this 4-to-1 contraction problem.

We next evaluate the effects of three physical parameters n, λ_c, and Re on corner vortex behaviors, viscosity contour behaviors, and the horizontal velocity component along the outlet and the axis of symmetry in the contraction plane. To evaluate how physical parameters affect the vortex upstream of the contraction plane, we varied $Re = 1$ and $Re = 10$, $\lambda_c = 1$ and $\lambda_c = 2$, and $n = 0.5$ and $n = 0.1$ in Fig. 6. For $Re = 1$ and $\lambda_c = 1$, Figs. 6(a) ($n = 0.5$) and 6(b) ($n = 0.1$) show that a decrease in n only causes a light decrease in the vortex upstream of the contraction plane. For $Re = 1$ and $n = 0.5$, Figs. 6(a) ($\lambda_c = 1$) and 6(c) ($\lambda_c = 2$) display that the sized of the corner vortex near the contraction is decreased as λ_c increases. To evaluate the

Please cite this article in press as: H.-C. Lee, A nonlinear weighted least-squares finite element method for the Carreau–Yasuda non-Newtonian model, J. Math. Anal. Appl. (2015), http://dx.doi.org/10.1016/j.jmaa.2015.07.012

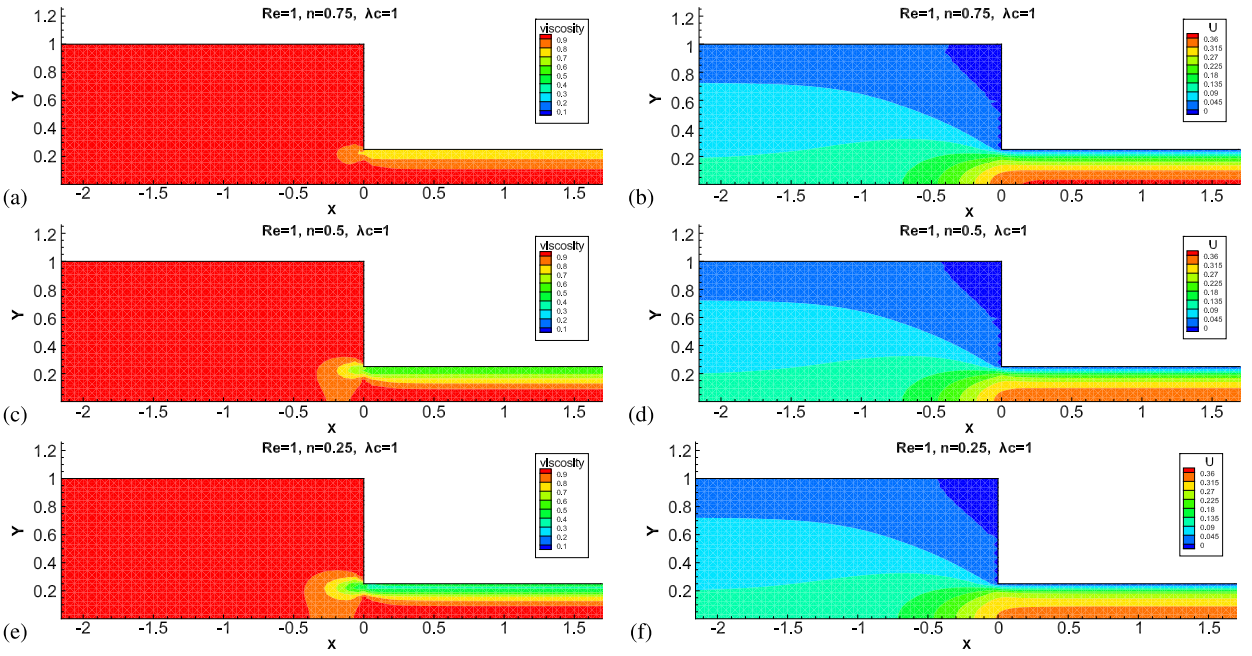

Fig. 7. $Re = 1$, $\lambda_c = 1$. Contours of the viscosity η at (a) $n = 0.75$, (c) $n = 0.5$, and (e) $n = 0.25$, and the horizontal velocity component u at (b) $n = 0.75$, (d) $n = 0.5$, and (f) $n = 0.25$. (For interpretation of the references to color in this figure legend, the reader is referred to the web version of this article.)

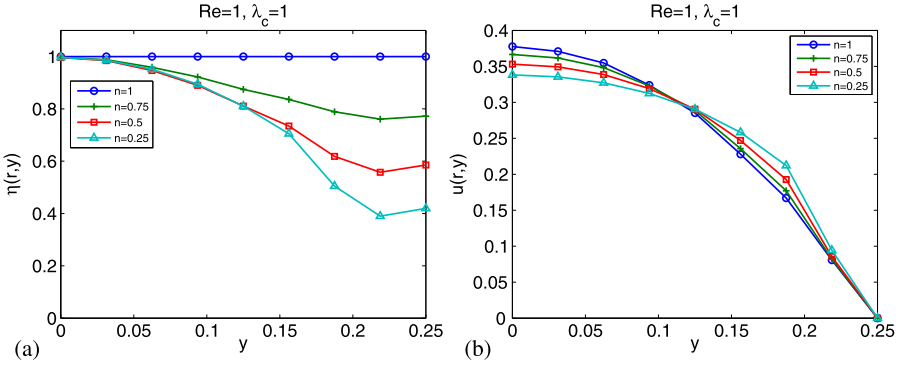

Fig. 8. $Re = 1$, $\lambda_c = 1$. Profiles of (a) the viscosity function $\eta(r, y)$ and (b) the horizontal velocity $u(r, y)$ along the outlet $r = 10$ at $n = 1$ (o), $n = 0.75$ (+), $n = 0.5$ (□), and $n = 0.25$ (△).

inertia effect, for $n = 0.5$ and $\lambda_c = 1$, Figs. 6(a) ($Re = 1$) and 6(d) ($Re = 10$) present an obvious decrease in the vortex upstream of the contraction plane as Re increases. The results show that the size of the corner vortex is decreased as n decreases, λ_c and Re increase.

Next, the physical parameter effects on the viscosity function η and the horizontal velocity component u are investigated. To evaluate the effects of the power-law index n, we employ $n = 0.75, 0.5,$ and 0.25 with $Re = 1$ and $\lambda_c = 1$ in Fig. 7. These figures show the contours of the viscosity η and the horizontal velocity u. Our results indicate a build up of boundary layers in the downstream of the reentrant corner, and the feature of the contour near the wall in the downstream becomes more obvious as indices n are decreased. Figs. 8(a) and 8(b) show the profiles of the viscosity function η and the horizontal velocity component u along the outlet, respectively. The results in Fig. 8(a) show that the viscosity of the fluids with $n < 1$ at the wall ($y = 0.25$) is lower than that at the axis of symmetry ($y = 0$). Because the low-index fluid near the wall has a low viscosity, the velocity growth rate away from the wall of the low-index fluid is greater than in the high-index fluid. To ensure mass conservation, in the axis of symmetry the velocity of the low-index

Please cite this article in press as: H.-C. Lee, A nonlinear weighted least-squares finite element method for the Carreau–Yasuda non-Newtonian model, J. Math. Anal. Appl. (2015), http://dx.doi.org/10.1016/j.jmaa.2015.07.012

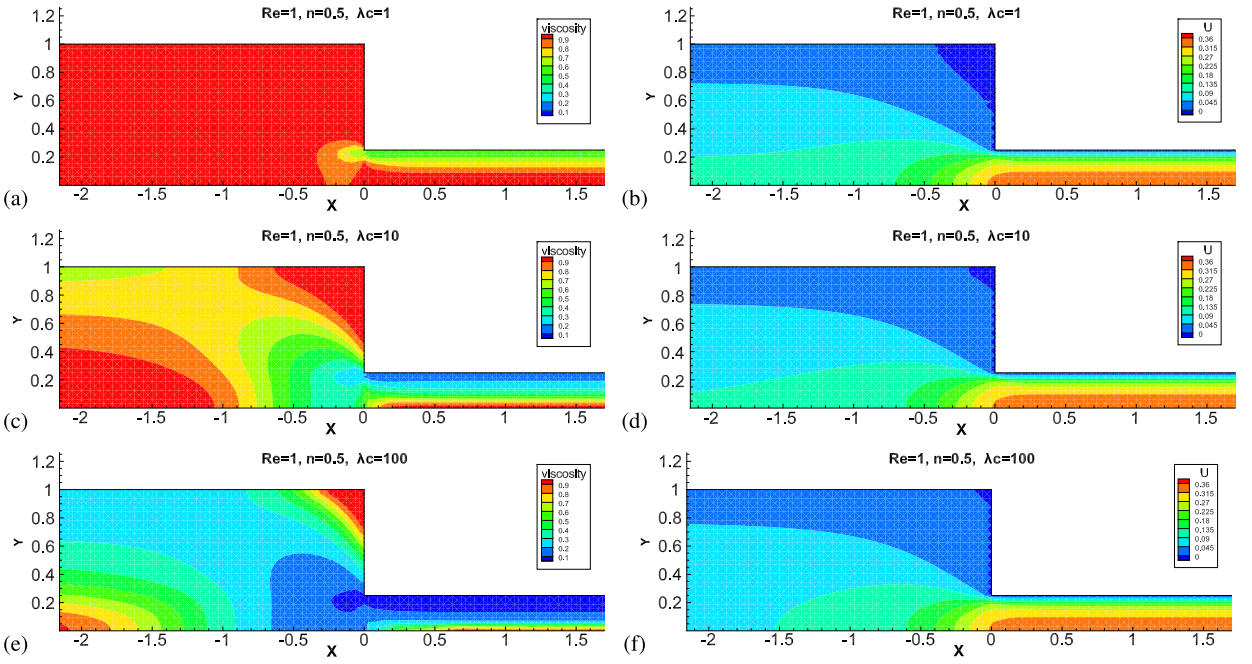

Fig. 9. $Re = 1$, $n = 0.5$. Contours of the viscosity η at (a) $\lambda_c = 1$, (c) $\lambda_c = 10$, and (e) $\lambda_c = 100$, and the horizontal velocity component u at (b) $\lambda_c = 1$, (d) $\lambda_c = 10$, and (f) $\lambda_c = 100$. (For interpretation of the references to color in this figure legend, the reader is referred to the web version of this article.)

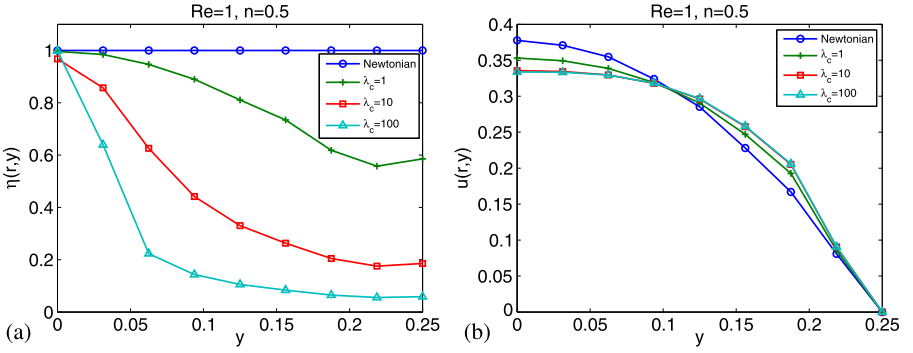

Fig. 10. $Re = 1$, $n = 0.5$. Profiles of (a) the viscosity function $\eta(r, y)$ and (b) the horizontal velocity $u(r, y)$ along the outlet $r = 10$ at the Newtonian model(o), $\lambda_c = 1$ (+), $\lambda_c = 10$ (□), and $\lambda_c = 100$ (△).

fluid is lower than in the high-index fluid, as shown in Fig. 8(b). The results show that when $n = 0.25$, the fluid velocity near the wall is higher than for other values of n and also causes the flattest velocity profile at the outlet. By decreasing n, the viscous effects become less dominant and these profiles become flatter. Further analysis of the viscosity data indicates that the feature of nonlinearity becomes more obvious as n decreases.

To evaluate the effects of the Carreau time number λ_c, $Re = 1$, and $n = 0.5$ are used. We employ $\lambda_c = 1$, 10, and 100 in Fig. 9. These figures show the contours of the viscosity η and the horizontal velocity u. The results show that the feature of the contour near the corner in the upstream becomes more obvious when λ_c is increased. Figs. 10(a) and 10(b) show the profiles of the viscosity function η and the horizontal velocity component u along the outlet, respectively. These results show that as λ_c increases, the feature of nonlinearity of the viscosity function η becomes more obvious and flattens the u profile. The velocity growth rate away from the wall of the high λ_c fluid is greater than that of the low λ_c fluid. The effect of increasing λ_c is similar to that of decreasing n. Note that according to the viscosity contour, the Carreau

Please cite this article in press as: H.-C. Lee, A nonlinear weighted least-squares finite element method for the Carreau–Yasuda non-Newtonian model, J. Math. Anal. Appl. (2015), http://dx.doi.org/10.1016/j.jmaa.2015.07.012

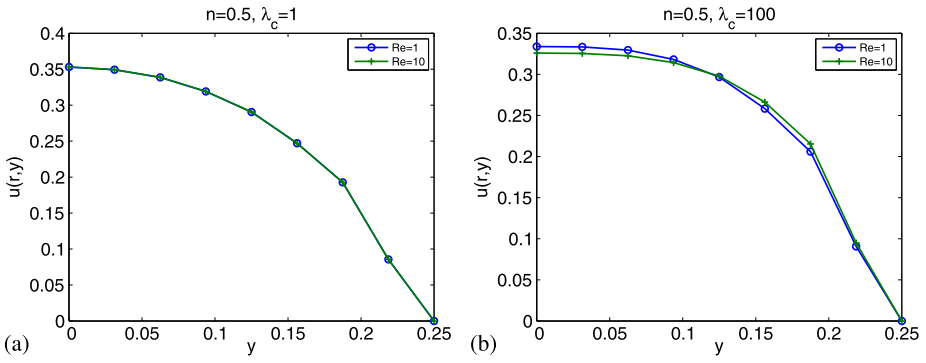

Fig. 11. Profiles of the velocity $u(r, y)$ along the outlet $r = 10$ for (a) $n = 0.5$, $\lambda_c = 1$ and (b) $n = 0.5$, $\lambda_c = 100$ at $Re = 1$ (o) and $Re = 10$ (+).

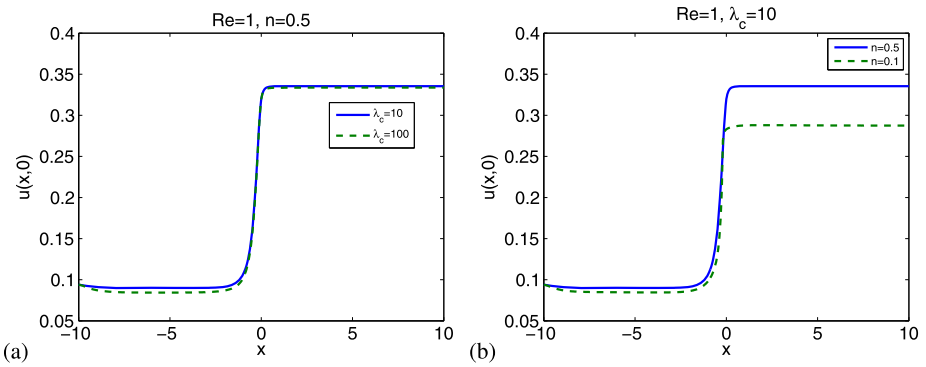

Fig. 12. Profiles of the velocity $u(x, 0)$ along the symmetric line. $Re = 1$ for (a) $n = 0.5$ with $\lambda_c = 10$ (line) and $\lambda_c = 100$ (dash line), and (b) $\lambda_c = 10$ with $n = 0.5$ (line) and $n = 0.1$ (dash line).

time number appears to be more sensitive to viscosity compared with the power-law indices, particularly in the upstream region of the contraction flow path. The effects of the power-law index and Carreau time number on the velocity field are similar to those observed by Zinani and Frey [17].

To evaluate the inertia effects, we employ $Re = 1$ and 10 in the Carreau model at $n = 0.5$, and two values of time numbers, $\lambda_c = 1$ and $\lambda_c = 100$ in Figs. 11(a) and 11(b), respectively. For the low Carreau time number ($\lambda_c = 1$), the same profiles of the horizontal velocity component u along the outlet are shown for various Re cases in Fig. 11(a), although the size of the vortex changes in Figs. 6(a) and 6(d). The figure results show that the inertia effects on the vortex near the corner are more obvious than the velocity profiles in the fully developed outlet. For the high Carreau time number ($\lambda_c = 100$, Fig. 11(b)), the growth rate of the velocity away from the wall of the high Re fluid is greater than in the low Re fluid. The results show that the high Carreau time number fluid at high Re may have affected velocity. For the high Carreau time fluid, the effects of Re become dominant and are similar to that of decreasing n. The effects of Re on the velocity field for a high Carreau time fluid are similar to those found by Reddy and Padhye [15] for a power-law fluid.

Fig. 12 shows the plots of $u(x, 0)$ along the symmetric line for the effects of different Carreau time numbers λ_c ($\lambda_c = 10$ and $\lambda_c = 100$, Fig. 12(a)) and indices n ($n = 0.5$ and $n = 0.1$, Fig. 12(b)). Fig. 12(a) shows that for the same Re and n, an increase in λ_c only causes a slight decrease in centerline velocity values upstream and almost overlaps the regions of fully developed flow. Fig. 12(b) shows that for the same Re and λ_c, a change in the n index strongly affects flow behavior, particularly downstream and near the contraction. Because of the high strain rates in these regions, a more flattened velocity profile is formed as n decreases. The results show that the index n effects in the centerline velocity values downstream are stronger than the Carreau time number λ_c effects.

Please cite this article in press as: H.-C. Lee, A nonlinear weighted least-squares finite element method for the Carreau–Yasuda non-Newtonian model, J. Math. Anal. Appl. (2015), http://dx.doi.org/10.1016/j.jmaa.2015.07.012

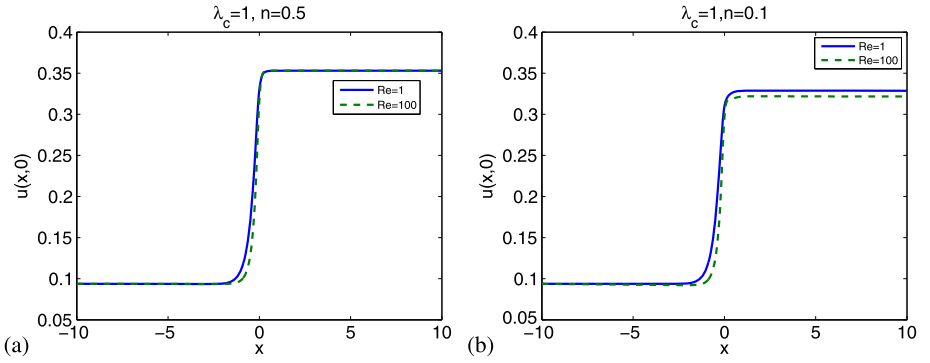

Fig. 13. Profiles of the velocity $u(x, 0)$ along the symmetric line. $Re = 1$ (line) and $Re = 100$ (dash line) for (a) $\lambda_c = 1$, $n = 0.5$, and (b) $\lambda_c = 1$, $n = 0.1$.

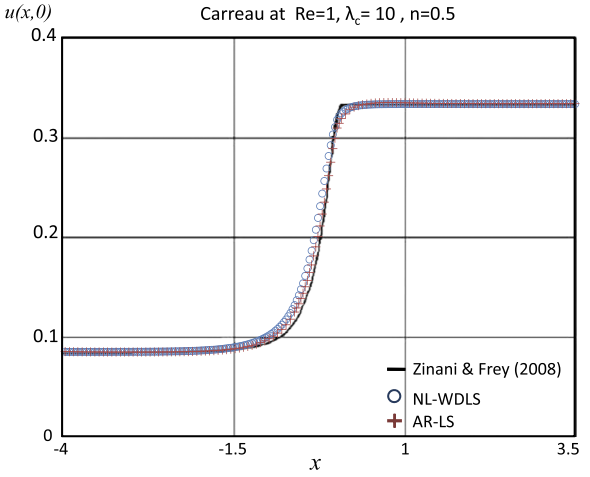

Fig. 14. Comparison between results of the NL-WDLS and the AR-LS, and those of Zinani and Frey. Profiles of the velocity $u(x, 0)$ along the symmetric line for $Re = 1$ at $\lambda_c = 10$, $n = 0.5$.

Fig. 13 shows the profiles of $u(x, 0)$ along the symmetric line for different Re numbers ($Re = 1$ and $Re = 100$) in the case of $\lambda_c = 1$, $n = 0.5$ (Fig. 13(a)) and $n = 0.1$ (Fig. 13(b)). For the high index $n = 0.5$ fluid (Fig. 13(a)), the maximum velocity in the regions of fully developed flow is the same for both Re. The main differences between the $Re = 1$ and $Re = 100$ cases occur near the contraction, because these regions are subjected to high strain rates. For the low-index $n = 0.1$ fluid (Fig. 13(b)), an increase in Re causes a slight decrease in centerline velocity values downstream and an increase in the entrance length for high Re. The Re number effects become more dominant for the case of low n. These results show that the NL-WDLS solutions agree with the shear-thinning physical behavior of a high shear rate near the channel wall causing low viscosity in the region. Because the physical parameters have a large exchange, a high shear rate is produced and a nonlinear phenomenon of the viscosity is more obvious. Therefore, the physical parameter effects become dominant for the case of the high nonlinear viscosity.

Fig. 14 displays a comparison between our NL-WDLS results with the AR-LS [12] and GLS results of Zinani and Frey [17] for the horizontal velocity u profiles along the symmetric line in the contraction plane for $Re = 1$, $\lambda_c = 10$, and $n = 0.5$. The figure shows that the profiles used in the NL-WDLS method are similar to those used in the AR-LS and GLS methods. Therefore, it is assumed that the results are in agreement.

Please cite this article in press as: H.-C. Lee, A nonlinear weighted least-squares finite element method for the Carreau–Yasuda non-Newtonian model, J. Math. Anal. Appl. (2015), http://dx.doi.org/10.1016/j.jmaa.2015.07.012

6. Conclusion

We present a NL-WDLS finite element approximation to the Carreau–Yasuda non-Newtonian model. Comparisons are made with various least-squares formulations such as LS, WDLS, and NL-WDLS. These results show that by using linear polynomials in all variables, the expected optimal convergence rates in numerical results can be restored with a careful choice of nonlinear weighting functions, and are superior to those theoretically predicted. In addition, we extended the NL-WDLS method to the 4-to-1 contraction problem and address the physical parameter effects. For flows in the planar contraction, the NL-WDLS method is able to capture shear-thinning features such as the flattening of the velocity profiles in the contraction plane because of decaying viscosity. For the case of high nonlinear viscosity, our results show that the effects of the power-law index and of the time number become dominant, and that the inertial term in the momentum equation cannot be neglected. These results agree with published AR-LS and GLS results. Furthermore, the NL-WDLS method is simpler to implement than the AR-LS and GLS methods. We will extend the approach to more physically realistic domains, including more complex geometries and higher *Re* non-Newtonian flows in the future.

References

[1] R.B. Bird, R.C. Armstrong, O. Hassager, Dynamics of Polymeric Liquids, Fluid Mech., vol. 1, John Wiley and Sons, New York, 1987.
[2] P.B. Bochev, M.D. Gunzburger, Finite element methods of least-squares type, SIAM Rev. 40 (1998) 789–837.
[3] P.B. Bochev, M.D. Gunzburger, Least-Squares Finite Element Methods, Springer, New York, 2009.
[4] A. Bose, G.F. Carey, Least-squares p-r finite element methods for incompressible non-Newtonian flows, Comput. Methods Appl. Mech. Engrg. 180 (1999) 431–458.
[5] J. Boyd, J.M. Buick, S. Green, Analysis of the Casson and Carreau–Yasuda non-Newtonian blood models in steady and oscillatory flows using the lattice Boltzmann method, Phys. Fluids 19 (2007) 093103.1–093103.14.
[6] Z. Cai, C.R. Westphal, An adaptive mixed least-squares finite element method for viscoelastic fluids of Oldroyd type, J. Non-Newtonian Fluid Mech. 159 (2009) 72–80.
[7] Z. Cai, T.A. Manteuffel, S.F. McCormick, First-order system least squares for second-order partial differential equations. II, SIAM J. Numer. Anal. 34 (1997) 425–454.
[8] T.F. Chen, C.L. Cox, H.C. Lee, K.L. Tung, Least-squares finite elements methods for generalized Newtonian and viscoelastic flows, Appl. Numer. Math. 60 (2010) 1024–1040.
[9] T.F. Chen, H. Lee, C.C. Liu, Numerical approximation of the Oldroyd-B model by the weighted least-squares/discontinuous Galerkin method, Numer. Methods Partial Differential Equations 29 (2013) 531–548.
[10] O.M. Coronado, D. Arora, M. Behr, M. Pasquali, Four-field Galerkin/least-squares formulation for viscoelastic fluids, J. Non-Newtonian Fluid Mech. 140 (2006) 132–144.
[11] H.C. Lee, A nonlinear weighted least-squares finite element method for the Oldroyd-B viscoelastic flow, Appl. Math. Comput. 219 (2012) 421–434.
[12] H.C. Lee, An adaptively refined least-squares finite element method for generalized Newtonian fluid flows using the Carreau model, SIAM J. Sci. Comput. 36 (2014) 193–218.
[13] H.C. Lee, Weighted least-squares finite element methods for the linearized Navier–Stokes equations, Int. J. Comput. Math. 91 (2014) 1964–1985.
[14] H.C. Lee, T.F. Chen, A nonlinear weighted least-squares finite element method for Stokes equations, Comput. Math. Appl. 59 (2010) 215–224.
[15] J.N. Reddy, V.A. Padhye, A penalty finite element model for axisymmetic flows of non-Newtonian fluids, Numer. Methods Partial Differential Equations 4 (1988) 33–56.
[16] S.S. Shibeshi, W.E. Collins, The rheology of blood flow in a branched arterial system, Appl Rheol. 15 (2005) 398–405.
[17] F. Zinani, S. Frey, Galerkin least-squares multifield approximations for flows of inelastic non-Newtonian fluids, J. Fluids Engrg. 130 (2008) 081507 (14 pages).

Please cite this article in press as: H.-C. Lee, A nonlinear weighted least-squares finite element method for the Carreau–Yasuda non-Newtonian model, J. Math. Anal. Appl. (2015), http://dx.doi.org/10.1016/j.jmaa.2015.07.012